

Twist-angle sensitivity of electron correlations in moiré graphene bilayersZachary A. H. Goodwin, Fabiano Corsetti, Arash A. Mostofi, and Johannes Lischner *Departments of Materials and Physics and the Thomas Young Centre for Theory and Simulation of Materials, Imperial College London, South Kensington Campus, London SW7 2AZ, United Kingdom*

(Received 6 May 2019; published 13 September 2019)

Motivated by the recent observation of correlated insulator states and unconventional superconductivity in twisted bilayer graphene, we study the dependence of electron correlations on the twist angle and reveal the existence of strong correlations over a narrow range of twist angles near the magic angle. Specifically, we determine the on-site and extended Hubbard parameters of the low-energy Wannier states using an atomistic quantum-mechanical approach. The ratio of the on-site Hubbard parameter and the width of the flat bands, which is an indicator of the strength of electron correlations, depends sensitively on the screening by the semiconducting substrate and the metallic gates. Including the effect of long-ranged Coulomb interactions significantly reduces electron correlations and explains the experimentally observed sensitivity of strong-correlation phenomena on twist angles.

DOI: [10.1103/PhysRevB.100.121106](https://doi.org/10.1103/PhysRevB.100.121106)

Introduction. The recent discovery of strong-correlation phenomena in magic-angle twisted bilayer graphene (tBLG), namely, unconventional superconductivity in proximity to insulator states [1–5], has generated tremendous interest [6–26]. The measured phase diagram of tBLG resembles that of cuprates [2,4], but the microscopic origin of the correlated states remains controversial [6–23]. tBLG offers unique advantages for studying strong electron correlations as it is highly tunable through the twist angle [27–29], hydrostatic pressure [3,30], doping, electric and magnetic fields, and temperature [1–5]. Experimental measurements on tBLG, however, are highly sample dependent, indicating a strong twist-angle sensitivity of strong-correlation phenomena [1–3,5].

tBLG consists of two vertically stacked graphene sheets that are rotated with respect to each other, resulting in a moiré pattern that is generally incommensurate but, for certain angles, exhibits long-range periodicity associated with the moiré superlattice [27–29,31,32]. Theoretical studies show that at a “magic” twist angle of $\sim 1.1^\circ$, around which the moiré unit cells associated with commensurate structures contain thousands of atoms, the width of the four bands near the Fermi level becomes very small [28,29], reflecting a reduction of the electronic kinetic energy. It is then expected that the ratio of the electron interaction energy to the electron kinetic energy increases, signaling the increasing dominance of electron-electron interactions and the emergence of strongly correlated electronic behavior [1–3,5]. Indeed, correlated-insulator states and unconventional superconductivity are found when the system is doped by integer numbers of electrons or holes per moiré unit cell [1–5].

To help understand the microscopic origins of strong-correlation phenomena in tBLG, a wide range of theoretical approaches have been used. Atomistic tight-binding calculations [29–31,33] and continuum models [26–28,34–41] have provided valuable insights into the band structure of tBLG, but do not capture the effect of electron correlations. The effects of electron-electron interactions have been studied using

quantum Monte Carlo [6–8], renormalization group [9–13], self-consistent Hartree-Fock [14], and other theoretical and computational approaches [15,18,21].

The material-specific parameters that enter the interacting low-energy Hamiltonians of tBLG are often expressed in a Wannier function basis [11,17]. Wannier functions (WFs) of tBLG have been constructed by Koshino *et al.* [26] using a continuum model and by Kang and Vafeek [24] within atomistic tight binding. These groups also used the WFs to calculate hopping parameters and Coulomb interaction matrix elements at a single twist angle near the magic angle [11,26].

In this Rapid Communication, we investigate the dependence of electron correlations in tBLG on the twist angle. In particular, we carry out atomistic tight-binding calculations for a set of twist angles and construct WFs for each twist angle to determine the matrix elements of the screened Coulomb interaction between electrons in the flat bands. We demonstrate that both screening and the long-ranged interaction drastically reduce the range of twist angles over which strong-correlation phenomena may be expected. Specifically, the range is found to be only 0.1° around the magic angle, in good agreement with experimental estimates [1–3].

Methods. To gain insights into the electronic structure of tBLG, we solve the atomistic tight-binding Hamiltonian given by

$$\hat{H}_0 = \sum_{i,j} \{t(\mathbf{r}_i - \mathbf{r}_j) \hat{c}_j^\dagger \hat{c}_i + \text{H.c.}\}, \quad (1)$$

where \hat{c}_i^\dagger and \hat{c}_i are, respectively, the creation and annihilation operators of electrons in p_z orbitals of atom i , and $t(\mathbf{r}_i - \mathbf{r}_j)$ is the hopping parameter between atoms i and j obtained using the Slater-Koster approach [29,31,42]. The effect of out-of-plane atomic corrugation [30,32,43–45] is included following Ref. [26]. See Supplemental Material (SM) [46] for additional details.

Figure 1(a) shows the tight-binding band structure of tBLG at a twist angle of 1.05° . In good agreement with the literature

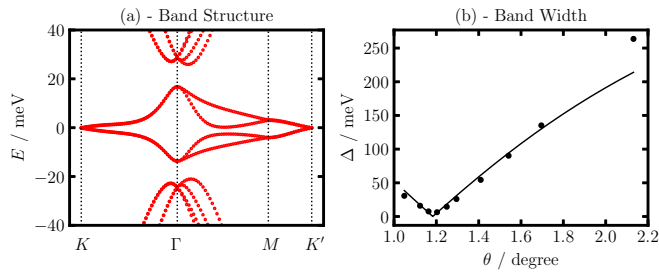


FIG. 1. (a) Atomistic tight-binding band structure for a twist angle of 1.05° (the Fermi level is at 0 meV). (b) Calculated bandwidth as a function of twist angle (dots) and analytical fit (solid black line).

[26,30,41,47,48], we find a set of four flat bands near the Fermi level. Figure 1(b) shows the width Δ of the flat bands as a function of the twist angle. The calculated bandwidths are accurately described by $\Delta = \delta [\theta^2 - (\theta^*)^2] / [\theta^2 + 2(\theta^*)^2]$ with a magic angle of $\theta^* = 1.18^\circ$ and $\delta = 0.5$ eV [28]. Note that θ^* is slightly larger than that found in previous continuum model results [28].

As the flat bands are separated from all other bands by energy gaps in the magic-angle regime, maximally localized Wannier functions (MLWFs) [49,50] can be constructed for these bands (without having to use a subspace selection procedure) according to

$$w_{n\mathbf{R}}(\mathbf{r}) = \frac{1}{\sqrt{N}} \sum_{m\mathbf{k}} e^{-i\mathbf{k}\cdot\mathbf{R}} U_{m\mathbf{k}} \psi_{m\mathbf{k}}(\mathbf{r}), \quad (2)$$

where $w_{n\mathbf{R}}$ is the WF and $\psi_{m\mathbf{k}}$ denotes a Bloch eigenstate of the Hamiltonian with band index m and crystal momentum \mathbf{k} ; $N = 30 \times 30$ is the number of \mathbf{k} points used to discretize the first Brillouin zone; \mathbf{R} is a moiré lattice vector; $U_{m\mathbf{k}}$ is a unitary matrix that mixes the Bloch bands at each \mathbf{k} and represents the gauge freedom of the Bloch states. To obtain MLWFs, $U_{m\mathbf{k}}$ is chosen such that the total quadratic spread of the resulting WFs is minimized [49,50].

To obtain a Wannier-transformed Hamiltonian that reproduces the symmetries of the band structure of tBLG, the WFs must be centered at the AB or the BA positions of the moiré unit cell [17,24–26] (shown in Fig. 2). We therefore use the approach of Ref. [51] and selectively localize two WFs and constrain the centers, one on each of these positions (see SM [46] for more details).

To calculate MLWFs (see SM [46] and Ref. [52]), it is expedient to choose an initial gauge by projecting the Bloch

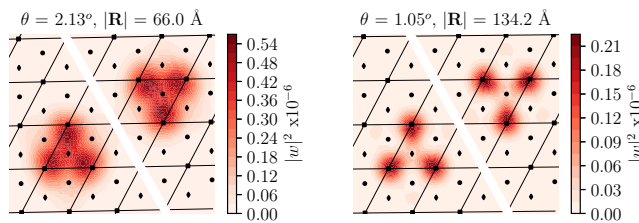


FIG. 2. Flat-band Wannier functions of tBLG with a twist angle of 2.13° (left) and 1.05° (right). Shown is the square modulus of the coefficients of the Wannier functions on each carbon atom. The squares, diamonds, and circles denote the centers of the AA, AB, and BA regions of tBLG, respectively.

states onto some trial guess for the WFs [49,50]. We tested two different starting guesses following suggestions from Refs. [24,26]. Both initial guesses produce MLWFs with nearly identical shapes and the resulting Coulomb matrix elements typically differ by less than 5% (see SM [46] for more details). In both cases, we obtain MLWFs using the WANNIER90 code (version 3.0) [53] with a custom interface to our in-house atomistic tight-binding code [54]. Figure 2 shows the resulting MLWFs for two twist angles. In agreement with previous work [17,24,26], we find the WFs exhibit three lobes that sit on the AA regions of the moiré unit cell.

In the Wannier basis, the interacting part of the Hamiltonian is given by

$$\hat{H}_{\text{int}} = \frac{1}{2} \sum_{\{n_i\mathbf{R}_i\}} V_{\{n_i\mathbf{R}_i\}} \hat{c}_{n_4\mathbf{R}_4}^\dagger \hat{c}_{n_3\mathbf{R}_3}^\dagger \hat{c}_{n_2\mathbf{R}_2} \hat{c}_{n_1\mathbf{R}_1}, \quad (3)$$

where $\hat{c}_{n\mathbf{R}}^\dagger$ and $\hat{c}_{n\mathbf{R}}$ are, respectively, the creation and annihilation operators of electrons in the Wannier state $|w_{n\mathbf{R}}\rangle$, and $V_{\{n_i\mathbf{R}_i\}}$ denotes a matrix element of the screened Coulomb interaction, $W(\mathbf{r} - \mathbf{r}')$. The largest matrix elements are usually obtained when $\mathbf{R}_4 = \mathbf{R}_1$, $\mathbf{R}_3 = \mathbf{R}_2$, $n_4 = n_1$, and $n_3 = n_2$. For this case, the Coulomb matrix element is given by

$$V_{ij} = \iint d\mathbf{r} d\mathbf{r}' |w_i(\mathbf{r})|^2 W(\mathbf{r} - \mathbf{r}') |w_j(\mathbf{r}')|^2. \quad (4)$$

We evaluate Eq. (4) for two models of the screened interaction. In the first case a Coulomb potential is used, $W(r) = e^2 / 4\pi\epsilon_r\epsilon_0 r$. The dielectric constant ϵ_r has contributions from the substrate [typically hexagonal boron nitride (hBN) [1–3]] and high-energy bands of tBLG. Values between 6 and 10 have been used in the literature [11,15]; here, we use $\epsilon_r = 8$.

In the second case, we include the effect of metallic gates on both sides of the tBLG (but separated from it by the hBN substrate). The resulting screened interaction is given by [55]

$$W^g(\mathbf{r} - \mathbf{r}') = \frac{e^2}{4\pi\epsilon_r\epsilon_0} \sum_{n=-\infty}^{+\infty} \frac{(-1)^n}{\sqrt{|\mathbf{r} - \mathbf{r}'|^2 + (\xi n)^2}}, \quad (5)$$

where $\xi = 10$ nm is half the distance between the two metallic gates [11,55]. For $|\mathbf{r} - \mathbf{r}'| \ll \xi$, W^g is proportional to the bare Coulomb interaction ($n = 0$ term). In the opposite limit, the interaction simplifies to $W^g(r) = \sqrt{2}e^2 e^{-\pi r/\xi} / (2\pi\epsilon_r\epsilon_0\sqrt{r\xi})$ [55]. See SM [46] for more details.

Results and discussion. The circle data points in Fig. 3(a) show the on-site Hubbard parameter V_{00} of tBLG without metallic gates as a function of the twist angle. In this range of twist angles, the on-site Hubbard parameters have values of approximately 25–50 meV, two orders of magnitude smaller than in graphene [56]. Moreover, we find that V_{00} depends approximately linearly on the twist angle, i.e., $V_{00} = (m_{00}\theta + c_{00})/\epsilon_r$, with $m_{00} = 200$ meV/degree and $c_{00} = 24$ meV. This dependence can be understood from the following scaling argument. If the decay length of the WF is proportional to the size of the moiré unit cell (and the WFs have no other twist-angle dependence), transforming the integrals in Eq. (4) to dimensionless coordinates immediately shows that V_{00} scales as the inverse size of the moiré unit cell length which is inversely proportional to θ in the limit of small twist angles.

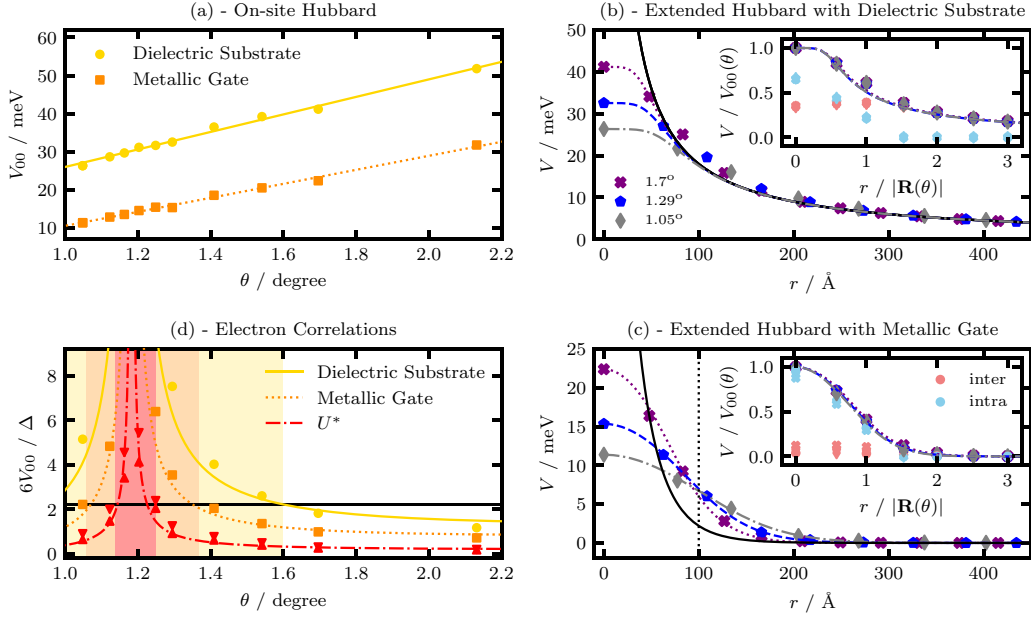


FIG. 3. (a) On-site Hubbard parameter in tBLG encapsulated by hBN as a function of twist angle for different models of the screened interaction. (b) Extended Hubbard parameters for tBLG on hBN as a function of distance between Wannier functions for three angles (1.70° , 1.29° , and 1.05°); dotted lines represent Eq. (6) and the solid line the dielectric screened Coulomb potential. Inset: Rescaled extended Hubbard parameters and contributions from intralobe (cyan symbols) and interlobe (pink symbols) contributions. (c) Extended Hubbard parameters for tBLG on hBN with metallic gates as a function of the distance between Wannier orbitals; dotted lines represent Eq. (7) and the solid line the large separation limit of Eq. (5). Inset: Rescaled extended Hubbard parameters and decomposition into intra- and interlobe contributions. (d) Ratio of the on-site Hubbard interaction to bandwidth in tBLG as a function of twist angle. Circles denote results for tBLG on hBN; squares denote results for tBLG on hBN with metallic gates; and triangles denote results for tBLG on hBN with (upwards facing triangle) and without (downwards facing triangle) metallic gates when extended Hubbard parameters are taken into account.

Including the screening from the metallic gates reduces the on-site Hubbard parameter by roughly a factor of 2 [see squares in Fig. 3(a)]. Again, we find a linear dependence of V_{00}^g on the twist angle with $m_{00}^g = 148$ meV/degree and $c_{00}^g = -63$ meV. This finding is surprising as the scaling argument applied to the screened interaction of Eq. (5) suggests that the resulting dimensionless integrals should be strong functions of θ . We expect that this nonlinear behavior would be seen over a larger range of twist angles than that studied here.

Figure 3(b) shows the extended Hubbard parameters of tBLG without metallic gates as a function of the separation between WF centers for three twist angles. The extended Hubbard parameters decay slowly as a function of distance as a consequence of the long-ranged Coulomb interaction and converge to the screened interaction evaluated at the Wannier centers for distances larger than four moiré unit cells [black solid line in Fig. 3(b)].

We fit our results for the extended Hubbard parameters (including the on-site term) to a modified Ohno potential [57]

$$V(r, \theta) = \frac{V_{00}(\theta)}{\sqrt[5]{1 + [V_{00}(\theta)/W(r)]^5}}. \quad (6)$$

Figure 3(b) shows, as seen with the dotted lines, that this expression accurately describes the calculated extended Hubbard parameters for *all twist angles* with only two parameters, m_{00} and c_{00} (see SM [46] for more details). The inset of Fig. 3(b) shows that the extended Hubbard parameters collapse onto a universal *twist-angle-independent* curve when the WF separation is divided by the moiré unit cell length $|\mathbf{R}(\theta)|$.

The inset of Fig. 3(b) also shows the contributions to the extended Hubbard parameters from intra- and interlobe interactions of the WFs [26]. The intralobe contributions decay to zero after second nearest neighbors, while the interlobe contributions initially increase (as a consequence of having more nonoverlapping lobe pairs) and then decay slowly.

Figure 3(c) shows that when screening from the metallic gates is taken into account, the extended Hubbard parameters decay to zero on a length scale of the order of the tBLG–gate distance, $\xi = 10$ nm (dotted vertical line). These extended Hubbard parameters can be accurately described by the modified Ohno potential of Eq. (6) multiplied by a Gaussian,

$$V^g(r, \theta) = \frac{V_{00}^g(\theta)e^{-(r/\alpha|\mathbf{R}(\theta)|)^2}}{\sqrt[5]{1 + [V_{00}^g(\theta)/W^g(r)]^5}}. \quad (7)$$

We find $\alpha \sim 1.1$ provides a good description of the data in the range of twist angles studied.

Again, the extended Hubbard parameters collapse onto a universal curve upon rescaling the distances, as shown in the inset of Fig. 3(c). The inset also shows that the extended Hubbard parameters are dominated by intralobe contributions as the finite range of W^g reduces the contribution from interlobe terms. This observation also explains the reduction of the on-site Hubbard parameter by a factor of 2 in the presence of metallic gates [Fig. 3(a)]: Without metallic gates, approximately half of V_{00} is contributed by interlobe interactions which are screened out by the gates.

Figure 3(d) shows the ratio of the on-site Hubbard parameter V_{00} to the bandwidth Δ as a function of twist angle for different screened interactions. Note that we have multiplied V_{00}/Δ by a factor of 6 to approximate V_{00}/t , which is typically used to characterize the strength of electronic correlations ($\Delta = 6t$ for graphene with nearest-neighbor hopping only [58]). As expected, V_{00}/t becomes large near the magic angle. The largest values of V_{00}/t are obtained for the screened interaction without metallic gates. Taking the screening from the metallic gates into account reduces V_{00}/t by approximately a factor of 2.

Our results thus demonstrate that electron correlations in tBLG can be continuously tuned as a function of twist angle from a weakly correlated to a strongly correlated regime in the vicinity of the magic angle. Calculating the phase diagram of such a system is extremely challenging as most theoretical approaches are tailored to one of the two limiting cases and are correspondingly classified as weak-coupling or strong-coupling techniques. Quite generally, it is expected that tBLG undergoes a metal-to-insulator transition as the strength of the electron correlations increases, but the detailed microscopic nature of the insulating phase remains controversial.

Mean-field theory and strong-coupling techniques predict that the gapped phase in undoped tBLG is an antiferromagnetic insulator [7,8,59,60]. However, the exact value of the critical V_{00}/t where the transition occurs has not been established. For (untwisted) Bernal stacked bilayer graphene, accurate quantum Monte Carlo calculations yield a critical value of $6V_{00}/\Delta = 2.2$ [6,61] [black horizontal line in Fig. 3(d)]. Without metallic gates, we find that the electronic correlations in tBLG exceed this critical value in a relatively large twist-angle range (from angles smaller than $\theta = 1.0^\circ$ up to $\theta = 1.6^\circ$). With metallic gates, the critical twist-angle range is reduced by over a factor of 2 (from $\theta = 1.06^\circ$ to $\theta = 1.37^\circ$).

In materials with significant, long-ranged Coulomb interactions, a different measure of strong correlations is appropriate. In particular, in such systems the energy gained by moving one electron from a doubly occupied orbital to a neighboring orbital is not V_{00} , but $U^* = V_{00} - V_{01}$ [62]. As U^* is about three (five) times smaller than V_{00} for the case of screening with (without) a metallic gate, long-range interactions drastically reduce the window of strongly correlated twist angles [see the red curve in Fig. 3(d) which is calculated from both interaction potentials studied here and found to be essentially independent of the type of interaction]. In particular, we find that the width of the critical twist-angle window is only 0.1° , which is in good agreement with recent experimental findings and explains the observed sensitivity of experimental measurements to sample preparation [1–3,5].

While gapped states in tBLG have been observed at charge neutrality [5], there is also significant interest in correlated insulator states of electron- or hole-doped systems [1–3,5]. Away from charge neutrality, weak-coupling approaches predict a transition from a metallic to a gapped antiferromagnetic phase at specific values of the Fermi level when the Fermi surface exhibits nesting with a critical value of $U^*/t \sim 2$ [9]. In contrast, strong-coupling calculations of doped tBLG predict that gapped *ferromagnetic* spin- or valley-polarized ground states occur whenever the number of additional carriers per moiré unit cell is integer [14]. This suggests the intriguing possibility that *multiple* phase transitions occur within the narrow, strongly correlated, twist-angle window.

Superconductivity in tBLG occurs at low temperatures in the vicinity of the correlated insulator phases [2,3,5]. While some works have suggested phonons as being responsible for the pairing mechanism [16,19], similarities to the cuprate phase diagram indicate that nonphononic mechanisms could be relevant in tBLG [9,12,13,60]. For example, superconductivity emerges in weak-coupling approaches from the exchange of damped spin waves [9,12,13]. Gonzalez and Stauber [12] have shown that very small values of U^*/t are sufficient to trigger superconductivity when the Fermi level lies near the van Hove singularity. This suggests that superconductivity could be observable in a larger twist-angle range than the correlated insulator phases.

Summary. We studied the twist-angle dependence of electron correlations in tBLG. For this, we calculated on-site and extended Hubbard parameters for a range of twist angles and demonstrated that the on-site Hubbard parameters depend linearly on the twist angle for both dielectric substrate and metallic gate screened interaction potentials. The extended Hubbard parameters decay slowly as a function of the Wannier function separation and are reproduced accurately *for all twist angles* with an Ohno-like potential. By calculating the ratio of the interaction energy and the kinetic energy of electrons in tBLG, we predict the twist-angle windows where strong-correlation phenomena occur. When the reduction of electron correlations arising from both screening and the long range of the electron interaction are taken into account, we find a critical twist-angle window of only 0.1° which explains the experimentally observed twist-angle sensitivity of strong-correlation phenomena in tBLG.

Acknowledgments. we thank V. Vitale, D. Kennes, C. Karasch, and A. Khedri for helpful discussions. This work was supported through a studentship in the Centre for Doctoral Training on Theory and Simulation of Materials at Imperial College London funded by the EPSRC (EP/L015579/1). We acknowledge funding from EPSRC Grant No. EP/S025324/1 and the Thomas Young Centre under Grant No. TYC-101.

- [1] Y. Cao, V. Fatemi, A. Demir, S. Fang, S. L. Tomarken, J. Y. Luo, J. D. Sanchez-Yamagishi, K. Watanabe, T. Taniguchi, E. Kaxiras, R. C. Ashoori, and P. Jarillo-Herrero, *Nature (London)* **556**, 80 (2018).
- [2] Y. Cao, V. Fatemi, S. Fang, K. Watanabe, T. Taniguchi, E. Kaxiras, and P. Jarillo-Herrero, *Nature (London)* **556**, 43 (2018).

- [3] M. Yankowitz, S. Chen, H. Polshyn, Y. Zhang, K. Watanabe, T. Taniguchi, D. Graf, A. F. Young, and C. R. Dean, *Science* **363**, 1059 (2019).
- [4] Y. Cao, D. Chowdhury, D. Rodan-Legrain, O. Rubies-Bigordà, K. Watanabe, T. Taniguchi, T. Senthil, and P. Jarillo-Herrero, *arXiv:1901.03710*.

- [5] X. Lu, P. Stepanov, W. Yang, M. Xie, M. A. Aamir, I. Das, C. Urgell, K. Watanabe, T. Taniguchi, G. Zhang, A. Bachtold, A. H. MacDonald, and D. K. Efetov, [arXiv:1903.06513](https://arxiv.org/abs/1903.06513).
- [6] H. Guo, X. Zhu, S. Feng, and R. T. Scalettar, *Phys. Rev. B* **97**, 235453 (2018).
- [7] Y. D. Liao, Z. Y. Meng, and X. Y. Xu, [arXiv:1901.11424](https://arxiv.org/abs/1901.11424).
- [8] X. Y., K. T. Law, and P. A. Lee, *Phys. Rev. B* **98**, 121406(R) (2018).
- [9] D. M. Kennes, J. Lischner, and C. Karrasch, *Phys. Rev. B* **98**, 241407(R) (2018).
- [10] Y. Sherkunov and J. J. Betouras, *Phys. Rev. B* **98**, 205151 (2018).
- [11] J. Kang and O. Vafek, *Phys. Rev. Lett.* **122**, 246401 (2019).
- [12] J. González and T. Stauber, *Phys. Rev. Lett.* **122**, 026801 (2019).
- [13] C.-C. Liu, L.-D. Zhang, W.-Q. Chen, and F. Yang, *Phys. Rev. Lett.* **121**, 217001 (2018).
- [14] M. Xie and A. H. MacDonald, [arXiv:1812.04213](https://arxiv.org/abs/1812.04213).
- [15] B. Padhi, C. Setty, and P. W. Phillips, *Nano Lett.* **18**, 6175 (2018).
- [16] Y. W. Choi and H. J. Choi, *Phys. Rev. B* **98**, 241412(R) (2018).
- [17] H. C. Po, L. Zou, A. Vishwanath, and T. Senthil, *Phys. Rev. X* **8**, 031089 (2018).
- [18] J. M. Pizarro, M. J. Calderón, and E. Bascones, *J. Phys. Commun.* **3**, 035024 (2019).
- [19] F. Wu, A. H. MacDonald, and I. Martin, *Phys. Rev. Lett.* **121**, 257001 (2018).
- [20] F. Wu, *Phys. Rev. B* **99**, 195114 (2019).
- [21] M. Ochi, M. Koshino, and K. Kuroki, *Phys. Rev. B* **98**, 081102(R) (2018).
- [22] B. Roy and V. Juričić, *Phys. Rev. B* **99**, 121407(R) (2019).
- [23] F. Guinea and N. R. Walet, *Proc. Natl. Acad. Sci. U.S.A.* **115**, 13174 (2018).
- [24] J. Kang and O. Vafek, *Phys. Rev. X* **8**, 031088 (2018).
- [25] N. F. Q. Yuan and L. Fu, *Phys. Rev. B* **98**, 045103 (2018).
- [26] M. Koshino, N. F. Q. Yuan, T. Koretsune, M. Ochi, K. Kuroki, and L. Fu, *Phys. Rev. X* **8**, 031087 (2018).
- [27] J. M. B. Lopes dos Santos, N. M. R. Peres, and A. H. Castro Neto, *Phys. Rev. Lett.* **99**, 256802 (2007).
- [28] R. Bistritzer and A. H. MacDonald, *Proc. Natl. Acad. Sci. U.S.A.* **108**, 12233 (2010).
- [29] G. T. de Laissardière, D. Mayou, and L. Magaud, *Nano Lett.* **10**, 804 (2010).
- [30] S. Carr, S. Fang, P. Jarillo-Herrero, and E. Kaxiras, *Phys. Rev. B* **98**, 085144 (2018).
- [31] G. Trambly de Laissardière, D. Mayou, and L. Magaud, *Phys. Rev. B* **86**, 125413 (2012).
- [32] K. Uchida, S. Furuya, J.-I. Iwata, and A. Oshiyama, *Phys. Rev. B* **90**, 155451 (2014).
- [33] E. Suárez Morell, J. D. Correa, P. Vargas, M. Pacheco, and Z. Barticevic, *Phys. Rev. B* **82**, 121407(R) (2010).
- [34] H. C. Po, L. Zou, T. Senthil, and A. Vishwanath, *Phys. Rev. B* **99**, 195455 (2019).
- [35] P. Moon and M. Koshino, *Phys. Rev. B* **87**, 205404 (2013).
- [36] E. J. Mele, *Phys. Rev. B* **81**, 161405(R) (2010).
- [37] E. J. Mele, *Phys. Rev. B* **84**, 235439 (2011).
- [38] G. Tarnopolsky, A. J. Kruchkov, and A. Vishwanath, *Phys. Rev. Lett.* **122**, 106405 (2019).
- [39] N. R. Walet and F. Guinea, [arXiv:1903.00340](https://arxiv.org/abs/1903.00340).
- [40] F. Guinea and N. R. Walet, *Phys. Rev. B* **99**, 205134 (2019).
- [41] S. Carr, S. Fang, Z. Zhu, and E. Kaxiras, *Phys. Rev. Research* **1**, 013001 (2019).
- [42] J. C. Slater and G. F. Koster, *Phys. Rev.* **94**, 1498 (1954).
- [43] A. Oshiyama, J.-I. Iwata, K. Uchida, and Y.-I. Matsushita, *J. Appl. Phys.* **117**, 112811 (2015).
- [44] F. Gargiulo and O. V. Yazyev, *2D Mater.* **5**, 015019 (2018).
- [45] S. K. Jain, V. Juricčić, and G. T. Barkema, *2D Mater.* **4**, 015018 (2017).
- [46] See Supplemental Material at <http://link.aps.org/supplemental/10.1103/PhysRevB.100.121106> for further calculation details, and tabulated parameters and fitted coefficients.
- [47] M. Angeli, D. Mandelli, A. Valli, A. Amaricci, M. Capone, E. Tosatti, and M. Fabrizio, *Phys. Rev. B* **98**, 235137 (2018).
- [48] J. Liu, J. Liu, and X. Dai, *Phys. Rev. B* **99**, 155415 (2019).
- [49] N. Marzari and D. Vanderbilt, *Phys. Rev. B* **56**, 12847 (1997).
- [50] N. Marzari, A. A. Mostofi, J. R. Yates, I. Souza, and D. Vanderbilt, *Rev. Mod. Phys.* **84**, 1419 (2012).
- [51] R. Wang, E. A. Lazar, H. Park, A. J. Millis, and C. A. Marianetti, *Phys. Rev. B* **90**, 165125 (2014).
- [52] K. W.-K. Shung, *Phys. Rev. B* **34**, 979 (1986).
- [53] G. Pizzi, V. Vitale, R. Arita, S. Blügel, F. Freimuth, G. Géranton, M. Gibertini, D. Gresch, C. Johnson, T. Koretsune, J. Ibanez-Azpiroz, H. Lee, D. Marchand, A. Marrazzo, Y. Mokrousov, J. I. Mustafa, Y. Nohara, Y. Nomura, L. Paulatto, S. Poncè, T. Ponweiser, J. Qiao, F. Thöle, S. Tsirkin, M. Wierzbowska, N. Marzari, D. Vanderbilt, I. Souza, A. A. Mostofi, and J. R. Yates, [arXiv:1907.09788](https://arxiv.org/abs/1907.09788), www.wannier90.org.
- [54] F. Corsetti, A. A. Mostofi, and J. Lischner, *2D Mater.* **4**, 025070 (2017).
- [55] R. E. Throckmorton and O. Vafek, *Phys. Rev. B* **86**, 115447 (2012).
- [56] T. O. Wehling, E. Şaşıoğlu, C. Friedrich, A. I. Lichtenstein, M. I. Katsnelson, and S. Blügel, *Phys. Rev. Lett.* **106**, 236805 (2011).
- [57] K. Ohno, *Theor. Chim. Acta* **2**, 219 (1964).
- [58] A. H. Castro Neto, F. Guinea, N. M. R. Peres, K. S. Novoselov, and A. K. Geim, *Rev. Mod. Phys.* **81**, 109 (2009).
- [59] L. A. Gonzalez-Arraga, J. L. Lado, F. Guinea, and P. San-Jose, *Phys. Rev. Lett.* **119**, 107201 (2017).
- [60] X. Gu, C. Chen, J. N. Leaw, E. Laksono, V. M. Pereira, G. Vignale, and S. Adam, [arXiv:1902.00029](https://arxiv.org/abs/1902.00029).
- [61] T. C. Lang, Z. Y. Meng, M. M. Scherer, S. Uebelacker, F. F. Assaad, A. Muramatsu, C. Honerkamp, and S. Wessel, *Phys. Rev. Lett.* **109**, 126402 (2012).
- [62] M. Schüler, M. Rösner, T. O. Wehling, A. I. Lichtenstein, and M. I. Katsnelson, *Phys. Rev. Lett.* **111**, 036601 (2013).